

Tau neutrino propagation and tau energy loss

Sharada Iyer Dutta

*Department of Physics and Astronomy,
State University of New York at Stony Brook,
Stony Brook, New York 11794 USA*

Yiwen Huang and Mary Hall Reno

Department of Physics and Astronomy, University of Iowa, Iowa City, Iowa 52242 USA

Electromagnetic energy loss of tau leptons is an important ingredient for eventual tau neutrino detection from high energy astrophysical sources. Proposals have been made to use mountains as neutrino converters, in which the emerging tau decays in an air shower. We use a stochastic evaluation of both tau neutrino conversion to taus and of tau electromagnetic energy loss. We examine the effects of the propagation for mono-energetic incident tau neutrinos as well as for several neutrino power-law spectra. Our main result is a parameterization of the tau electromagnetic energy loss parameter β . We compare the results from the analytic expression for the tau flux using this β with other parameterizations of β .

I. INTRODUCTION

The observed neutrino fluxes in solar neutrino experiments [1] and in atmospheric neutrino experiments [2] lead to a picture of neutrino oscillations with substantial $\nu_\mu \rightarrow \nu_\tau$ mixing [3]. For high energies over astronomical distances, astrophysical sources of ν_e and ν_μ can become sources of ν_τ as well. One method of detecting ν_τ from astrophysical sources is to look for the charged particles they produced in or near neutrino telescopes.

Because of the short lifetime of the tau, $\nu_\tau \rightarrow \tau \rightarrow \nu_\tau$ regeneration can be an important effect as the ν_τ passes through a significant column depth through the Earth [4, 5, 6, 7, 8]. This is typically relevant for neutrino energies below $E_\nu \sim 10^8$ GeV. At higher energies, one can imagine using the Earth as a tau neutrino converter [8, 9, 10, 11, 12, 13, 14, 15, 16, 17, 18, 19]. Because of the relatively short interaction length of the neutrino at high energies, column depths on the order of the distance through a mountain or from small skimming angles relative to the horizon are most important. Following the tau neutrino conversion, a tau is detected by its decay e.g., in ice with IceCube, RICE or the proposed ANITA detectors, or after it emerges into the air. The possibility of detectable signals depends on the incident fluxes, of which there are a variety of models [20], and on the detectors and their sensitivity to various energy regimes.

Theoretical calculations often rely on approximating the neutrino interaction and tau energy loss in terms of analytic functions of energy and column depth [11, 12]. These analytic tools are important in exploring the possibility for tau neutrino signals in a variety of detectors, even though ultimately a full simulation of tau production and energy loss is required. In the energy regime where $E_\nu \gg 10^8$ GeV Huang, Tseng and Lin have made an evaluation of the smearing of energy due to tau propagation by doing an approximate stochastic evaluation of electromagnetic energy loss of the tau [19]. Looking at fixed incident neutrino energies, they find that the rel-

ative energy fluctuation of the tau can become large at high energies, especially for larger column depths. This has the potential to make interpretation of fluxes difficult at high energies.

In this paper, we evaluate tau neutrino and tau propagation using a stochastic evaluation of tau electromagnetic energy loss based on the work of Ref. [21]. We find the approximate evaluation of Ref. [19] reliable. In addition to considering mono-energetic incident neutrinos, we also consider incident neutrino fluxes with a power law behavior, $E_\nu^{-\gamma}$. We compare the flux of taus following propagation through 10 km rock and 100 km rock using the stochastic evaluation with estimates of the emerging flux of taus using analytic approximations. We refine some recent parameterizations of the tau energy loss as a function of tau energy [11, 12] to better approximate the stochastic result for the flux of emerging taus using analytic approximations. The best parameterization of the electromagnetic energy loss parameter β is with a logarithmic dependence on tau energy.

In the next section, we describe the models for the high energy neutrino nucleon cross section and the tau energy loss used in our Monte Carlo simulation. Results of the simulation and analytic approximations for the tau energy as a function of distance traveled, for monoenergetic neutrinos, appear in Section III. Section IV includes results and analytic approximations for power law incident neutrino spectra. A summary of our results and a comparison with a simplified analytic approach are in the final section.

II. NEUTRINO INTERACTIONS AND TAU ENERGY LOSS

Our evaluation of neutrino interactions and tau energy loss is performed using a one-dimensional Monte Carlo computer simulation. The neutrino charged current and neutral current interactions are calculated based on neutrino-isoscalar nucleon cross sections [22, 23] using

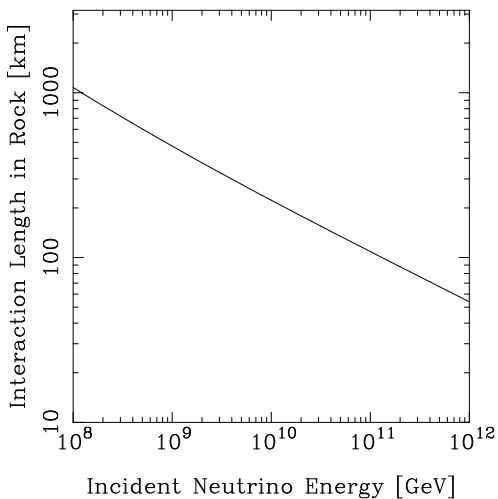


FIG. 1: Neutrino interaction length L_{int} in rock as a function of neutrino energy.

the CTEQ6 parton distribution functions (PDFs)[24].

At ultra-high energies, there is a competing effect in the neutrino-nucleon cross section as a function of $Q^2 = -q^2 > 0$, the quantity describing the four-momentum squared of the vector boson. PDFs increase as a function of $\ln Q^2$ [25], however, the vector boson propagator effectively cuts off the growth in Q^2 at the vector boson mass. For charged current scattering, this means that the value of parton $x \equiv Q^2/2p \cdot q$ for nucleon four-momentum p is approximately

$$x \sim \frac{M_W^2}{ME_\nu} \quad (1)$$

in terms of the incident neutrino energy E_ν , nucleon mass M and W boson mass M_W . For $E_\nu = 10^{12}$ GeV, one finds that $x \sim 10^{-8}$.

The CTEQ6 PDFs are parameterized for $10^{-6} < x < 1$, so one must extrapolate for smaller values of x . The PDFs at small values of parton x ($x < 10^{-6}$) are extrapolated here using a power law $xq(x, Q^2) \sim x^{-\lambda}$ matched to DGLAP evolved PDFs at $x_{\text{min}} = 10^{-6}$:

$$xq(x_{\text{min}}, M_W^2) = Ax_{\text{min}}^{-\lambda}. \quad (2)$$

This approach is based on the result [26] that for $\lambda \sim 0.3 - 0.4$, the gluon PDF has the approximate form of $xg(x, Q) \sim x^{-\lambda}$, and $g \rightarrow q\bar{q}$ splitting is responsible for the sea quark distributions that dominate the cross section at ultra-high energies. We show in Fig. 1 the neutrino interaction length in rock. Other approaches to the small x extrapolations for ultra-high energy neutrino cross sections yield similar interaction lengths [27], to within a factor of approximately $2^{\pm 1}$ at 10^{12} GeV.

The differential distribution for neutrino nucleon scattering in terms of the lepton inelasticity y ,

$$y \equiv \frac{E_\nu - E_\tau^i}{E_\nu}, \quad (3)$$

is evaluated similarly. We indicate the energy of the tau at the point of its production by E_τ^i . The neutrino interaction probability and resulting tau energy is evaluated using a one-dimensional Monte Carlo program. In our analytic approximations described below, we use $\langle y \rangle \simeq 0.2$, which is approximately correct at ultra-high energies [22]. An indication of this is shown by the solid line in Fig. 2, which shows the ratio of the average tau energy to the initial neutrino energy, as a function of neutrino energy, in the absence of electromagnetic energy loss corrections.

Our evaluation of the tau electromagnetic energy loss follows the procedure described in Ref. [21]. Based on the scheme outlined by Lipari and Stanev [28] and others [29], we have incorporated the electromagnetic mechanisms of ionization, bremsstrahlung (brem), e^+e^- pair production (pair) and photonuclear (nuc) scattering. The tau lifetime is taken into account.

The average energy lost per unit distance is commonly described by the formula

$$\left\langle \frac{dE_\tau}{dz} \right\rangle = -(\alpha + \beta E_\tau)\rho. \quad (4)$$

In this expression, z is the distance the tau travels. The quantity $\alpha \simeq 2 \times 10^{-3}$ GeV cm²/g accounts for ionization energy loss [30]. Here, β is

$$\begin{aligned} \beta &= \beta^{\text{brem}} + \beta^{\text{pair}} + \beta^{\text{nuc}} \\ &= \sum_i \frac{N_A}{A} \int dy y \frac{d\sigma^i}{dy}, \end{aligned} \quad (5)$$

for Avogadro's number N_A , atomic mass number A , tau inelasticity y and $i = \text{brem, pair and nuc}$.

In our treatment here, as in Ref. [21] we separate β into continuous and stochastic terms:

$$\begin{aligned} \beta &= \beta_{\text{cont}} + \beta_{\text{stoc}} \\ &= \frac{N_A}{A} \int_0^{10^{-3}} dy y \frac{d\sigma^i}{dy} + \frac{N_A}{A} \int_{10^{-3}}^1 dy y \frac{d\sigma^i}{dy}. \end{aligned} \quad (6)$$

We treat the tau propagation stochastically, with a series of electromagnetic interactions occurring according to probabilities based on $d\sigma^i/dy$ for $y > 10^{-3}$ and the decay probability. For each distance between interactions in the Monte Carlo program, the tau energy loss calculated from Eq. (3) is supplemented by Eq. (4) with the substitution of $\beta \rightarrow \beta_{\text{cont}}$. By doing it this way, we account for the full electromagnetic energy loss, but we limit computer time spent where the cross section is large, but the energy loss is small ($y < 10^{-3}$). The detailed formulas for the bremsstrahlung [31], pair production [32] and photonuclear [33] processes are discussed and collected in Ref. [21]. See also Ref. [34] for the muon case.

For the muon, β is dominated by pair production and bremsstrahlung for $E_\mu = 10^3 - 10^7$ GeV. At higher energies, β grows slowly with energy due to the photonuclear process which contributes a larger fraction for $E_\mu > 10^7$

GeV. For the tau, the photonuclear process is comparable to pair production, while the bremsstrahlung contribution is suppressed, leading to an increase in β with energy for $E_\tau > 10^3$ GeV.

In the analytic approximations discussed below, we will consider several forms of β as a function of E_τ , and we will treat

$$\left\langle \frac{dE_\tau}{dz} \right\rangle \simeq \frac{dE_\tau}{dz} . \quad (7)$$

To guide our discussion, it is useful to compare the relevant constants and distance scales. First, at 10^8 GeV,

$$\beta E_\tau \simeq 60 \frac{\text{cm}^2 \text{GeV}}{\text{g}} \left(\frac{E_\tau}{10^8 \text{ GeV}} \right) \quad (8)$$

is much larger than α , so we can essentially ignore α . The tau range is then characterized roughly by

$$\frac{1}{\beta \rho} \sim 6 \text{ km} \quad (9)$$

in standard rock ($\rho = 2.65 \text{ g/cm}^3$). In fact, the range is somewhat larger than this estimate. The decay length of the tau is

$$\gamma c \tau \simeq 5 \text{ km} \left(\frac{E_\tau}{10^8 \text{ GeV}} \right) . \quad (10)$$

It is in the energy regime near 10^8 GeV that the transition from the lifetime dominated to the energy loss dominated range for the tau occurs.

III. MONO-ENERGETIC NEUTRINOS

A. Results from Monte Carlo simulation

We begin our discussion by considering single incident neutrino energies to see the effect of energy loss combined with decay probabilities for two different trajectories: through 10 km rock (26.5 km.w.e.) and through 100 km rock. Fig. 2 shows the average tau energy divided by the incident neutrino energy as a function of incident neutrino energy. The average distance that the tau travels after production which survives to emerge from the rock (10, 50 and 100 km) is shown in Fig. 3.

For 10 km of rock, above 10^9 GeV, the average distance the tau travels is 5 km. The neutrino interaction probability is equal anywhere in the 10 km path, and the energies are large enough that the decay length is long compared to the path. For 50 km and 100 km, Fig. 3 shows that the last ~ 15 km are the most important for the emerging taus.

The standard deviation, normalized by the average tau energy,

$$\frac{\sigma}{E_\tau^{avg}} = \frac{\sqrt{\langle E_\tau^2 \rangle - \langle E_\tau \rangle^2}}{\langle E_\tau \rangle} \quad (11)$$

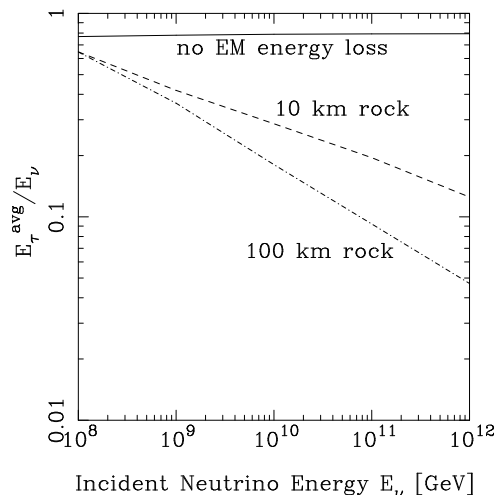


FIG. 2: Average tau energy scaled by the energy of incident neutrinos that produced the taus, without energy loss (solid), and with energy loss for taus produced in 10 km and 100 km rock (dashed).

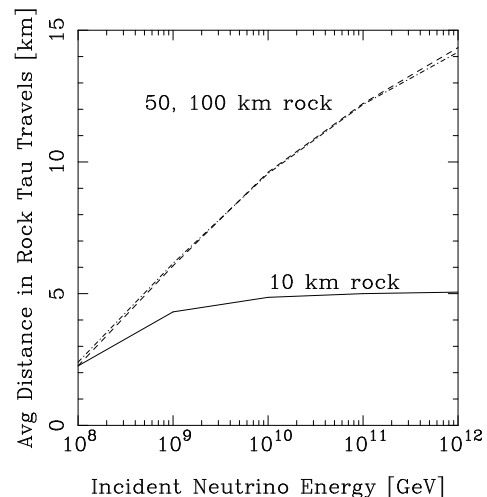


FIG. 3: Average distance the tau travels after production which survives to emerge from 10 km rock (solid), 50 km rock (dashed) and 100 km rock (dot-dashed), as a function of incident neutrino energy.

is shown in Fig. 4. Higher energies and larger distances lead to larger fluctuations. Huang et al.'s results in Ref. [19] correspond to our Figs. 2 and 4 and are in good agreement. We comment that by normalizing the standard deviation to the incident neutrino energy rather than average energy of the emerging tau, one finds a more stable result for the ratio. The standard deviation scales approximately as $(0.20 - 0.25) \times E_\nu$ for 10 km rock over the same energy range as the figure, and with a factor of $(0.13 - 0.25) \times E_\nu$ for 100 km rock.

A final result for mono-energetic neutrinos is shown in Fig. 5. Each histogram shows the average energy of the

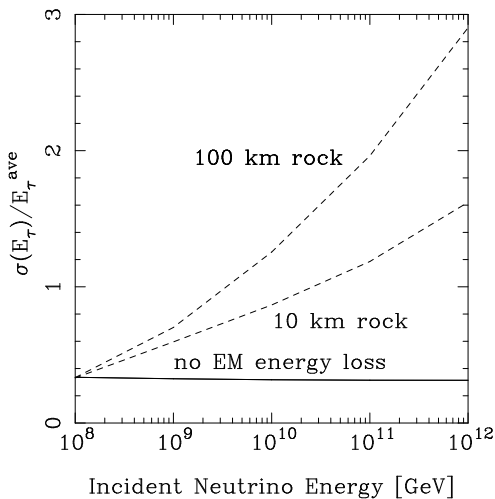


FIG. 4: Standard deviation σ scaled by the average tau energy as a function of the incident neutrino energy without energy loss (solid) and for 10 km and 100 km of rock (dashed).

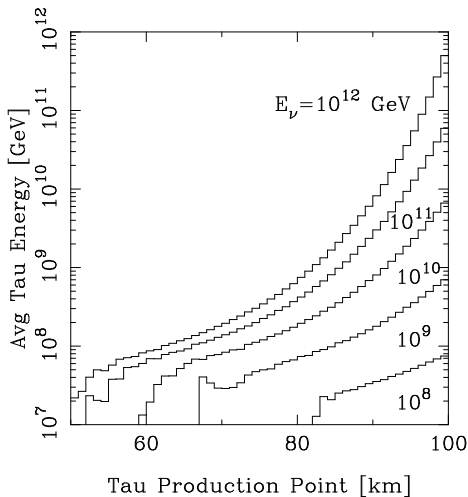


FIG. 5: Average energy of emerging tau as a function of its production point for a total distance of 100 km of rock, for fixed initial neutrino energies between $10^8 - 10^{12}$ GeV.

emerging tau as a function of the production point z for a total depth of 100 km and at fixed initial neutrino energy. The energies of the incident neutrinos are $E_\nu = 10^n$ GeV for $n = 8, 9, \dots, 12$ (lower to upper curves).

B. Analytic approximations

Standard approaches to parameterizing the final energy in terms of the initial energy begin with

$$\frac{dE_\tau}{dz} \simeq -\beta\rho E_\tau \quad (12)$$

The solution depends on the energy dependence of β . Several parameterizations have been used, including a linear dependence on energy [12] and a logarithmic energy dependence [8]. We consider three cases:

$$\begin{aligned} \text{(I)} \quad E_\tau &= E_\tau^i e^{-\beta\rho z'} \\ \beta &= \text{constant} \\ \text{(II)} \quad E_\tau &= \frac{E_\tau^i \beta_\tau e^{-\beta_\tau \rho z'}}{\beta_\tau + \gamma_\tau E_\tau^i (1 - e^{-\beta_\tau \rho z'})} \\ \beta &= \beta_\tau + \gamma_\tau E_\tau \quad (13) \\ \text{(III)} \quad E_\tau &= \exp\left[-\frac{\beta_0}{\beta_1}(1 - e^{-\beta_1 \rho z'})\right. \\ &\quad \left. + \ln(E_\tau^i/E_0) e^{-\beta_1 \rho z'}\right] E_0 \\ \beta &= \beta_0 + \beta_1 \ln(E/E_0) . \end{aligned}$$

The quantity z' is the distance traveled by the tau after its production. None of the choices for β is entirely satisfactory. Case (III) is the best approximation to the energy curves of Fig. 6. For case (I),

$$\beta = 0.85 \times 10^{-6} \text{ cm}^2/\text{g} \quad (14)$$

works moderately well for $E_\nu = 10^{10}$ GeV, but poorly for higher and lower energies. We reproduce the histograms of the stochastic results from Fig. 5 showing the last 20 km in Fig. 6 together with parameterizations of β . In all cases of the parameterized energy, we take $E_\tau^i = 0.8E_\nu$. The dot-dashed lines show the parameterization of case (I).

Case (II) is used by Aramo et al. in Ref. [12] with

$$\begin{aligned} \beta_\tau &= 0.71 \times 10^{-6} \text{ cm}^2/\text{g} \\ \gamma_\tau &= 0.35 \times 10^{-18} \text{ cm}^2/\text{g GeV} . \end{aligned} \quad (15)$$

The energy parameterization in this case is shown with the dashed lines in Fig. 6.

The parameterization using a logarithmic dependence on energy for β does the best at reproducing the energy behavior of the emerging taus. This is shown with solid lines in Fig. 6, with

$$\begin{aligned} \beta_0 &= 1.2 \times 10^{-6} \text{ cm}^2/\text{g} \\ \beta_1 &= 0.16 \times 10^{-6} \text{ cm}^2/\text{g} \\ E_0 &= 10^{10} \text{ GeV} . \end{aligned} \quad (16)$$

Not surprisingly, this energy dependent β will give the best representation of the Monte Carlo simulation results for the emerging tau fluxes from power law incident neutrino fluxes. We note that these values of β are larger than what one would extract from the direct calculation of β [21] as in Eq. (6). This is because Eq. (7) is only an approximate equality.

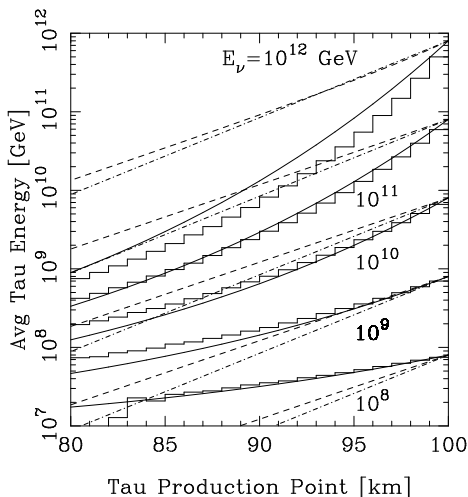


FIG. 6: Average energy of emerging tau as a function of its production point for a total distance of 100 km of rock, for fixed initial neutrino energies between $10^8 - 10^{12}$ GeV from Monte Carlo simulation (histograms), and parameterization of β as in case (I) (dot-dashed), case (II) (dash) and case (III) (solid).

IV. POWER LAW NEUTRINO SPECTRA

A. Results from Monte Carlo simulation

In this section, we consider cases of incident neutrino fluxes that depend on energy. Rather than use specific flux models, we consider power law fluxes $F_\nu \sim E_\nu^{-n}$, for $n = 1, 2, 3$, to see qualitatively and quantitatively how flux propagation is affected by tau energy loss.

In Fig. 7, we show the results of the stochastic propagation of the incident tau neutrino, which converts to a tau and continues through the depth D of rock, for $D = 10$ km and 100 km and an incident neutrino flux scaling like E_ν^{-1} . All of the fluxes shown in this section have a sharp cutoff at $E_\nu = 10^{12}$ GeV. The two upper dashed curves show the outgoing tau flux to the incoming neutrino flux neglecting tau energy loss and decay. Because of the larger column depth for 100 km of rock, the ratio of the tau to neutrino flux is ten times larger than for 10 km. The flux ratio increases with energy to scale with the neutrino cross section.

Our stochastic propagation including energy loss and decay is shown by the histograms in Fig. 7. Energy loss is much stronger for the 100 km depth, so the ratio of outgoing tau flux to incident neutrino flux is smaller for 100 km than 10 km for $E > 10^9$ GeV, despite the increased number of targets for the neutrinos. A qualitative discussion of the results for Fig. 7 is in Sec. IV.B.

Figs. 8 and 9 show the ratio of the outgoing tau flux to the incident tau neutrino flux for incident neutrino fluxes scaling as E_ν^{-2} and E_ν^{-3} , respectively. The flux ratios including decay and energy loss at $E = 10^8$ GeV for these steeper fluxes can be understood based only on

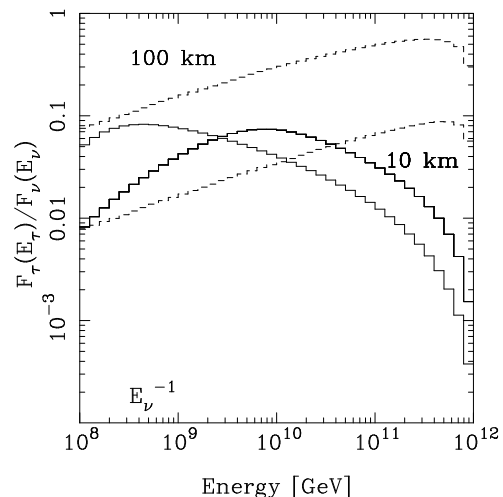


FIG. 7: Flux ratio of tau flux to incident neutrino flux as a function of energy for 10 km and 100 km of rock, for an incident neutrino energy scaling like E_ν^{-1} . The dashed lines do not have energy loss or decay included. The histograms include the stochastic treatment of the neutrino interaction and tau energy loss and decay.

the lifetime, since energy loss is not overwhelming at that energy and there is little pile-up of taus from neutrino interactions at higher energies, followed by tau energy loss. The dashed lines have a factor of D to account for the column depth of nucleon targets in the neutrino interaction probability. When decays are included, the relevant distance at $E = 10^8$ GeV is $d = E_\tau c\tau/m_\tau$, so the neutrino interaction probability is proportional to d rather than D . Neutrino attenuation in 10 km and 100 km of rock at $E_\nu \sim 10^8$ GeV is small, so the flux ratios in Figs. 8 and 9 are the same for the two depths. At higher energies, attenuation and energy loss play a bigger role.

Our aim here is to compare the stochastic propagation to analytic approaches. In the next section we outline the analytic evaluation of the emerging tau flux and make quantitative comparisons with the histograms in Fig. 7, 8 and 9.

B. Analytic approximations

The analytic approximation to the emerging tau flux as a function of tau energy depends on a number of components. We review the discussion of Ref. [11] here, expanded to include two energy dependences of β , a linear dependence [12] and a logarithmic one [8].

The incident flux $F_\nu(E_\nu, 0)$ is attenuated along its trajectory a distance z through the rock with an approximate factor

$$F_\nu(E_\nu, z) \simeq \exp\left[-z\sigma_{tot}(E_\nu)\rho NA\right]F_\nu(E_\nu, 0). \quad (17)$$

In our evaluation here, we are assuming a constant density (standard rock). Neutrino regeneration[4, 5, 6, 7, 8].

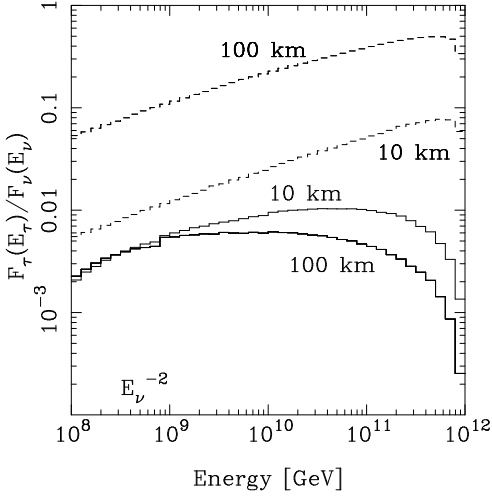


FIG. 8: Flux ratio of tau flux to incident neutrino flux as a function of energy for 10 km and 100 km of rock, for an incident neutrino energy scaling like E_ν^{-2} . The dashed histograms do not have energy loss or decay included. The histograms include the stochastic treatment of the neutrino interaction and tau energy loss and decay.

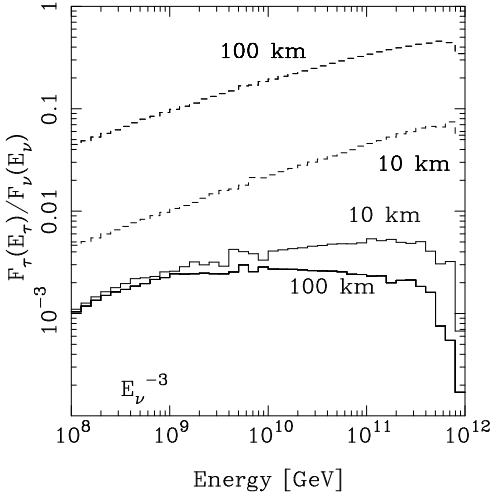


FIG. 9: Flux ratio of tau flux to incident neutrino flux as a function of energy for 10 km and 100 km of rock, for an incident neutrino energy scaling like E_ν^{-3} . The dashed lines do not have energy loss or decay included. The histograms include the stochastic treatment of the neutrino interaction and tau energy loss and decay.

from neutral current processes or tau decay is not important over these short distances.

The probability for neutrino conversion to taus in the distance interval $[z, z + dz]$ with energy in the interval $[E_\tau^i, E_\tau^i + dE_\tau^i]$ is

$$P_{CC}(\nu_\tau \rightarrow \tau, E_\nu, E_\tau^i) = dz dE_\tau^i N_A \rho \frac{d\sigma_{CC}(E_\nu, E_\tau^i)}{dE_\tau^i}. \quad (18)$$

As discussed above, we take $E_\tau^i = 0.8E_\nu$:

$$\frac{d\sigma_{CC}}{dE_\tau^i} \simeq \sigma_{CC}(E_\nu) \delta(E_\tau^i - (1 - \langle y \rangle) E_\nu) \quad (19)$$

$$\langle y \rangle \simeq 0.2. \quad (20)$$

Writing the differential cross section this way ensures that the integral over tau energy yields the charged-current (CC) cross section.

In the infinite lifetime, no energy loss ($\tau \rightarrow \infty, \beta \rightarrow 0$) limit, the emerging tau flux given incident tau neutrinos is

$$\begin{aligned} F_\tau(E_\tau^i)_{\tau \rightarrow \infty, \beta \rightarrow 0} &= \int_0^D dz \int dE_\nu N_A \rho \frac{d\sigma_{CC}(E_\nu, E_\tau^i)}{dE_\tau^i} \\ &\times \exp[-z\sigma_{tot}(E_\nu)\rho N_A] F_\nu(E_\nu, 0) \\ &\equiv \int_0^D dz \frac{dF_\tau^0(E_\tau^i, z)}{dz} \end{aligned} \quad (21)$$

for rock depth D .

In the case where the energy loss is treated analytically, the lifetime and energy loss are accounted by a factor $P_{surv}(E_\tau^i, E_\tau, D - z)$ as the tau travels over the remaining distance from production point z to emerge from the rock after distance D with outgoing energy E_τ . In fact, E_τ^i, E_τ and $D - z$ are not all independent, as shown in Eq. (13). The survival probability as a function of energy comes from the solution to the equation

$$\frac{dP_{surv}}{dz} = -\frac{P_{surv}}{c\tau E_\tau/m_\tau} \quad (22)$$

together with the approximate dE_τ/dz formula of Eq. (12), leading to

$$\frac{dP_{surv}}{dE_\tau} \simeq \frac{m_\tau}{c\tau\beta\rho E_\tau^2} P_{surv}. \quad (23)$$

The solution depends on the energy dependence of β . For constant β , the solution is

$$P_{surv}(E_\tau, E_\tau^i) = \exp\left[-\frac{m_\tau}{c\tau\beta\rho} \left(\frac{1}{E_\tau} - \frac{1}{E_\tau^i}\right)\right] \quad \text{case (I)}. \quad (24)$$

The emerging tau flux is

$$\begin{aligned} F_\tau(E_\tau) &= \int_0^D dz \frac{dF^0(E_\tau^i, z)}{dz} P_{surv}(E_\tau, E_\tau^i) \\ &\times \delta(E_\tau^i - E_\tau^i(E_\tau, D - z)) \frac{dE_\tau^i}{dE_\tau} dE_\tau^i \\ &= \int_0^D dz \frac{dF^0(E_\tau^i, z)}{dz} P_{surv}(E_\tau, E_\tau^i) \\ &\times \delta(E_\tau - E_\tau(E_\tau^i, D - z)) dE_\tau^i. \end{aligned} \quad (25)$$

The delta function explicitly enforces Eq. (13) rewritten with E_τ^i in terms of E_τ and $D - z$. A factor of dE_τ^i/dE_τ

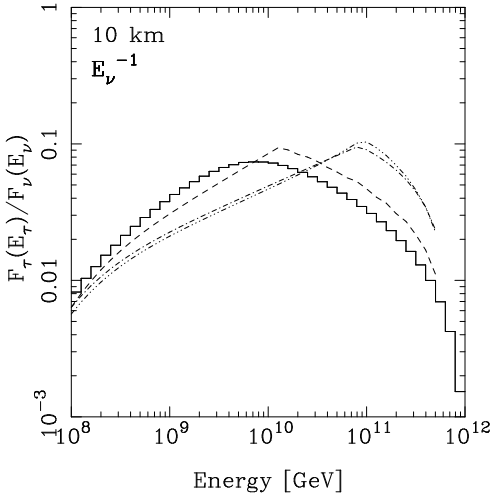


FIG. 10: Flux ratio of tau flux to incident neutrino flux as a function of energy for 10 km of rock, for an incident neutrino energy scaling like E_ν^{-1} . The histograms include the stochastic treatment of the neutrino interaction and tau energy loss and decay. The analytic approximations for cases (I, dot-dashed), (II, dot-dot-dot-dashed) and (III, dashed) are also shown.

accounts for the fact that $F_\tau(E_\tau)$ represents the number of τ 's per tau energy interval, say for $\Delta E_\tau = E_2 - E_1$. Electromagnetic energy loss means that one must sample a much larger interval of initial tau energies, $\Delta E_\tau^i = E_2 \exp(\beta\rho D) - E_1$. Combining this factor with the delta function leads to the factor of $\delta(E_\tau - E_\tau^i \exp(-\beta\rho(D-z)))$ that appears in the literature[11] for tau neutrino production of taus for a constant beta:

$$F_\tau(E_\tau) = \int_0^D dz \frac{dF^0(E_\tau^i, z)}{dz} P_{surv}(E_\tau, E_\tau^i) \times \delta(E_\tau - E_\tau^i \exp(-\beta\rho(D-z))) dE_\tau^i. \quad (26)$$

In the $\beta \rightarrow 0$ limit, the emerging tau flux is the expected result,

$$F_\tau(E_\tau) = \int_0^D dz \frac{dF^0(E_\tau^i, z)}{dz} \exp\left(-\frac{m_\tau(D-z)}{c\tau E_\tau}\right). \quad (27)$$

Continuing with case (I) for non-zero β , explicit substitutions give

$$F_\tau(E_\tau) = \int_0^D dz \int dE_\nu \exp(-z\sigma_{tot}(E_\nu)\rho N_A) F_\nu(E_\nu, 0) \times N_A \rho \sigma_{CC}(E_\nu) \delta(E_\tau - 0.8E_\nu \exp(-\beta\rho(D-z))) \times \exp\left[-\frac{m_\tau}{c\tau\beta\rho} \left(\frac{1}{E_\tau} - \frac{e^{-\beta\rho(D-z)}}{E_\tau}\right)\right]. \quad (28)$$

A useful limit to understand our results in Fig. 7 is the case of constant β in the long lifetime limit. For simplicity, we set $\langle y \rangle = 0$ so that $E_\tau^i = E_\nu$ [11]. If we also

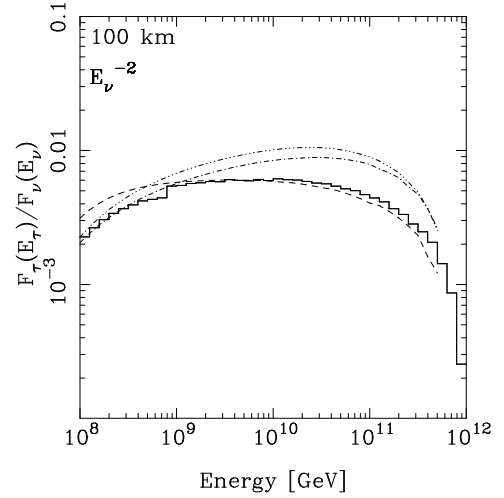


FIG. 11: Flux ratio of tau flux to incident neutrino flux as a function of energy for 100 km of rock, for an incident neutrino energy scaling like E_ν^{-2} . The histograms include the stochastic treatment of the neutrino interaction and tau energy loss and decay. The analytic approximations for cases (I, dot-dashed), (II, dot-dot-dot-dashed) and (III, dashed) are also shown.

assume $D \ll L_{int}$ where L_{int} is the neutrino interaction length, we can simplify Eq. (28) to

$$F_\tau(E_\tau) = \int_0^D \frac{dz}{L_{int}^{CC}} \int dE_\nu F_\nu(E_\nu, 0) \delta(E_\tau - E_\nu e^{-\beta\rho(D-z)}) = \frac{1}{E_\tau \beta \rho L_{int}^{CC}} \int_{E_{min}}^{E_{max}} dE_\nu F_\nu(E_\nu, 0), \quad (29)$$

for L_{int} approximately constant. The energy integral runs from $E_{min} = E_\tau$ to $E_{max} = \min(E_\tau \exp(\beta\rho D), 10^{12} \text{ GeV})$. At low energies and short distances, (e.g., $E_\tau \sim 10^8 \text{ GeV}$ and $D = 10 \text{ km}$), the maximum energy is $E_\tau \exp(\beta\rho D)$. For $F_\nu \sim E_\nu^{-1}$, $F_\tau \sim (D/L_{int}^{CC}) \cdot E_\tau^{-1}$, while for $F_\nu \sim E_\nu^{-n}$ for $n > 1$, $F_\tau \sim 1/((n-1)\beta\rho L_{int}^{CC}) \cdot E_\tau^{-n}$. This means that even with strong energy loss effects, for an E_ν^{-1} flux in the appropriate energy regime, the total distance D determines the tau flux rather than the characteristic scale of the energy loss, $1/\beta\rho$. In the actual case of the τ , the tau decay length $\gamma c\tau$ is comparable to the energy loss scale $1/\beta\rho$ at $E = 10^8 \text{ GeV}$. For the E_ν^{-1} flux, D is still the dominant scale, although the details including both energy loss and decay as well as energy dependent cross sections have an effect, as seen in Fig. 7. Figs. 8 and 9 show that this is not the case for E_ν^{-2} and E_ν^{-3} .

Eq. (25) is the master equation for all three cases discussed here for the three parameterizations of β . The argument of the delta function comes from Eq. (13) for the specific cases I-III. The survival probabilities come from the solution to Eq. (23) for the appropriate energy

dependent β . This gives (see Ref. [12] for case (II))

$$\begin{aligned}
 P_{surv}(E_\tau, E_\tau^i) &= \left(\frac{E_\tau^i(\beta_\tau + \gamma_\tau E_\tau)}{E_\tau(\beta_\tau + \gamma_\tau E_\tau^i)} \right)^{\frac{m_\tau \gamma_\tau}{c\tau \beta_\tau^2 \rho}} \\
 &\times \exp \left[-\frac{m_\tau}{c\tau \beta_\tau \rho} \left(\frac{1}{E_\tau} - \frac{1}{E_\tau^i} \right) \right] \quad \text{case (II)} \\
 P_{surv}(E_\tau, E_\tau^i) &= \exp \left(\frac{m_\tau \beta_1}{c\tau \rho \beta_0^2} \left[\frac{1}{E_\tau} \left(1 + \ln \left(\frac{E_\tau}{E_0} \right) \right) \right. \right. \\
 &\quad \left. \left. - \frac{1}{E_\tau^i} \left(1 + \ln \left(\frac{E_\tau^i}{E_0} \right) \right) \right] \right) \\
 &\times \exp \left[-\frac{m_\tau}{c\tau \beta_0 \rho} \left(\frac{1}{E_\tau} - \frac{1}{E_\tau^i} \right) \right] \quad \text{case (III)}.
 \end{aligned} \tag{30}$$

In case (III), an expansion in β_1/β_0 has been made in Eq. (23). Numerically, we have kept terms through β_1^3/β_0^3 , however in Eq. (30), we show the result where only the first term has been kept.

None of the parameterizations can completely describe the Monte Carlo results. Based on Fig. 6, it is not surprising that the form of β which depends on $\log E_\tau/E_0$ works the best to describe the outgoing tau flux. In Figs. 10-12, we show a comparison of the various parameterizations of the outgoing tau flux, normalized to the incident neutrino flux.

Fig. 10 shows the Monte Carlo results for 10 km of rock and an incident flux with E_ν^{-1} energy behavior with the histogram and the case (III) parameterization with the dashed line. The case (I) parameterization, with constant β appears as a dot-dashed line, while the case (II) power law is shown with a dot-dot-dot-dashed line. One sees the turnover in the flux ratio as the change is made from $E_{max} = E_\tau \exp(\beta \rho D)$ to $E_{max} = 10^{12}$ GeV for the E_ν^{-1} flux. The parameterization of β as a function of $\log(E_\tau/E_0)$ (case (III)) gives results for the flux ratio to within about $\pm 50\%$ of the Monte Carlo result. The other two parameterizations do not do as well, underestimating by a factor of ~ 2 for $E = 10^9$ GeV and overestimating by ~ 3 for $E = 10^{11}$ GeV.

For 100 km of rock, with the same incident flux, the case (III) parameterization compares well (underestimates by $\sim 15\%$) the Monte Carlo result between $10^9 - 10^{11}$ GeV. By comparison, the other two parameterizations for 100 km rock overestimate the tau flux by a factor of 1.3 – 1.6 and 1.8 – 2 at energies 10^{10} and 10^{11} GeV respectively.

For the E_ν^{-2} incident neutrino flux, the $\log E$ parameterization of β does well for 100 km as seen in Fig. 11. Again, the dot-dashed and dot-dot-dot-dashed lines show cases (I) and (II) respectively. For incident neutrino fluxes scaling with E_ν^{-3} , the 10 km result is well represented by the $\log E$ parameterization, as shown in Fig. 12. The overestimate of the flux for cases I and II occurs because energy loss is underestimated at high

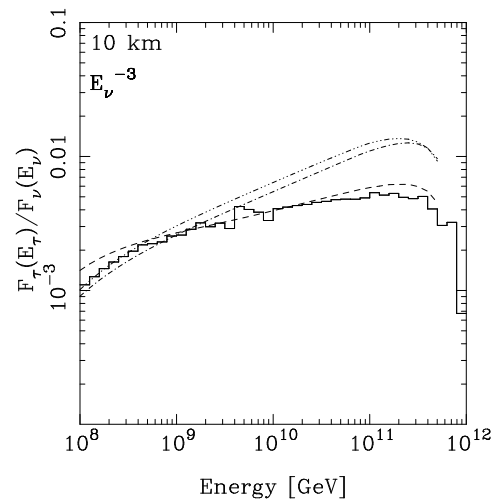


FIG. 12: Flux ratio of tau flux to incident neutrino flux as a function of energy for 10 km of rock, for an incident neutrino energy scaling like E_ν^{-3} . The histograms include the stochastic treatment of the neutrino interaction and tau energy loss and decay. The analytic approximations for cases (I, dot-dashed), (II, dot-dot-dot-dashed) and (III, dashed) are also shown.

energies with these parameterizations of β .

V. DISCUSSION

We have performed a one-dimensional Monte Carlo simulation of ν_τ conversion to τ and τ propagation including electromagnetic energy loss over distances of 10-100 km in rock. Analytic approximations are useful tools in exploring the possibility of detecting a variety of predictions for incident neutrino fluxes [11]. Using monoenergetic sources of tau neutrinos, we modeled the tau energy loss with an energy loss parameter β depending on $\log(E_\tau/E_0)$. In an analytic approximation for the outgoing tau flux, this model for energy loss does better at representing the Monte Carlo results than two other choices for β : a constant and a β increasing linearly with tau energy. Our improved parameterization of β will help refine theoretical predictions of tau neutrino induced events in neutrino telescopes.

It is not difficult to numerically evaluate the integrals of Eq. (25) including the more complicated logarithmic dependence on energy of β (case (III)) for P_{surv} and E_τ , nevertheless, it is interesting to see the impact of the modifications from that energy dependence. Although formally inconsistent, one could simply use the flux calculation for constant β , Eq. (26), and substitute $\beta = \beta_0 + \beta_1 \ln(E_\tau/E_0)$. This is shown in Fig. 13, for $D = 100$ km and E_ν^{-1} , with the dot-dashed line. As in Figs. 10-12, the dashed line comes from the full case III (logarithmic dependence) result, and the histogram represents the Monte Carlo result. The dot-dashed line

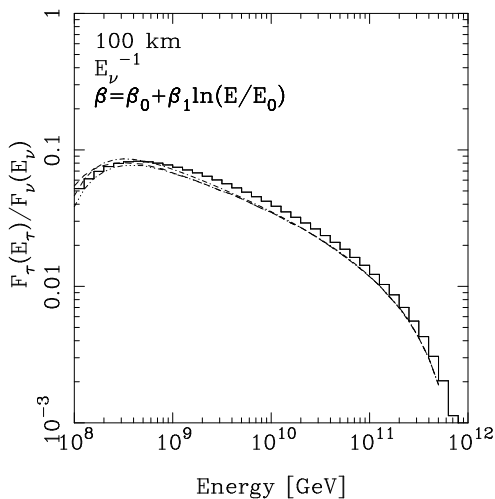


FIG. 13: Flux ratio of tau flux to incident neutrino flux as a function of energy for 100 km of rock, for an incident neutrino energy scaling like E_ν^{-1} . The histogram includes the stochastic treatment of the neutrino interaction and tau energy loss and decay. The analytic approximations using Eq. (28) with $\beta = \beta_0 + \beta_1 \ln(E/E_0)$ (dot-dashed), using $E_\tau(E_\tau^i, D - z)$ for case III but a simplified P_{surv} (triple dot-dashed) and the full case III result (dashed) also shown.

is nearly identical to the complete case III evaluation. The triple dot-dashed line uses the full expression for

the energy dependence on distance from Eq. (13), but it uses the simplified form of the survival probability: $P_{surv} = \exp[-m_\tau/(c\tau\beta\rho) \cdot (E_\tau^{-1} - E_\tau^i^{-1})]$. This does as well in representing the Monte Carlo result. Of the fluxes and rock depths that we have discussed here, Fig. 13 is representative of the three curves incorporating to varying degrees the logarithmic energy dependence of β .

In summary, our Monte Carlo results for tau neutrino interaction and tau propagation through rock suggest that the tau electromagnetic energy loss parameter be parameterized by $\beta = \beta_0 + \beta_1 \log(E/E_0)$ (case III), where the parameters β_0 , β_1 and E_0 appear in Eq. (16). Using the analytic formula of Ref. [11], modified to account for the logarithmic energy dependence, a reasonable agreement with the Monte Carlo results is obtained. Using the formulae of Ref. [11] for constant β , with the small change of taking $\langle y \rangle = 0.2$ but substituting $\beta(E_\tau)$, also is in reasonable agreement with the Monte Carlo result.

Acknowledgments

We thank I. Sarcevic and D. Seckel who were collaborators in our initial evaluation of tau electromagnetic energy loss, and T. Gaisser, K. Gayley, Y. Meurice and V.G.J. Rodgers. This work is funded in part by the U.S. Department of Energy contract DE-FG02-91ER40664.

-
- [1] S. N. Ahmed *et al.* [SNO Collaboration], Phys. Rev. Lett. **92**, 181301 (2004).
 - [2] Y. Ashie *et al.* [Super-Kamiokande Collaboration], Phys. Rev. Lett. **93**, 101801 (2004).
 - [3] M. C. Gonzalez-Garcia and M. Maltoni, hep-ph/0406056.
 - [4] F. Halzen and D. Saltzberg, Phys. Rev. Lett. **81**, 4305 (1998).
 - [5] S. I. Dutta, M. H. Reno and I. Sarcevic, Phys. Rev. D **62**, 123001 (2000).
 - [6] F. Becattini and S. Bottai, Proceedings of the International Cosmic Ray Conference, Salt Lake City 1999, Vol. 2, pp. 249-252 and Astropart. Phys. **15**, 323 (2001); S. Bottai and S. Giurgola, Astropart. Phys. **18**, 539 (2003).
 - [7] E. Bugaev, T. Montaruli, Y. Shlepin and I. Sokalski, Astropart. Phys. **21**, 491 (2004).
 - [8] D. Fargion, Astrophys. J. **570**, 909 (2002); astro-ph/9704205.
 - [9] S. Yoshida, R. Ishibashi and H. Miyamoto, Phys. Rev. D **69**, 103004 (2004).
 - [10] K. Giesel, J. H. Jureit and E. Reya, Astropart. Phys. **20**, 335 (2003).
 - [11] J. L. Feng, P. Fisher, F. Wilczek and T. M. Yu, Phys. Rev. Lett. **88**, 161102 (2002).
 - [12] C. Aramo, A. Insolia, A. Leonardi, G. Miele, L. Perrone, O. Pisanti and D. V. Semikoz, Astropart. Phys. **23**, 65 (2005).
 - [13] D. Fargion, astro-ph/0412582, astro-ph/0106239, hep-ph/0206010; D. Fargion, P. G. De Sanctis Lucentini and M. De Santis, Astrophys. J. **613**, 1285 (2004) and astro-ph/0501033;
 - [14] X. Bertou, P. Billoir, O. Deligny, C. Lachaud and A. Letessier-Selvon, Astropart. Phys. **17**, 183 (2002).
 - [15] H. Athar, G. Parente and E. Zas, Phys. Rev. D **62**, 093010 (2000).
 - [16] J. Jones, I. Mocioiu, M. H. Reno and I. Sarcevic, Phys. Rev. D **69**, 033004 (2004).
 - [17] P. Yeh *et al.* [NuTel Collaboration], Mod. Phys. Lett. A **19**, 1117 (2004).
 - [18] Z. Cao, M. A. Huang, P. Sokolsky and Y. Hu, astro-ph/0411677.
 - [19] M. A. Huang, J. J. Tseng and G. L. Lin, *Proceedings of 28th International Cosmic Ray Conferences (ICRC 2003)*, Tsukuba, Japan, 31 Jul - 7 Aug 2003 pp. 1427-1430.
 - [20] See, e.g., F. Halzen and D. Hooper, Rept. Prog. Phys. **65**, 1025 (2002) and references therein.
 - [21] S. I. Dutta, M. H. Reno, I. Sarcevic and D. Seckel, Phys. Rev. D **63**, 094020 (2001).
 - [22] R. Gandhi, C. Quigg, M. H. Reno and I. Sarcevic, Astropart. Phys. **5**, 81 (1996); G. M. Frichter, D. W. McKay and J. P. Ralston, Phys. Rev. Lett. **74**, 1508 (1995) [Erratum-ibid. **77**, 4107 (1996)].
 - [23] R. Gandhi, C. Quigg, M. H. Reno and I. Sarcevic, Phys. Rev. D **58**, 093009 (1998).
 - [24] J. Pumplin, D. R. Stump, J. Huston, H. L. Lai, P. Nadol-

- sky and W. K. Tung, *JHEP* **0207**, 012 (2002).
- [25] Yu. M. Andreev, V. S. Berezinsky and A. Yu. Smirnov, *Phys. Lett. B* **143**, 521 (1978).
- [26] R. K. Ellis, Z. Kunszt and E. M. Levin, *Nucl. Phys. B* **420**, 517 (1994).
- [27] M. Gluck, S. Kretzer and E. Reya, *Astropart. Phys.* **11**, 327 (1999); J. Kwiecinski, A. Martin and A. Stasto, *Phys. Rev. D* **56**, 3991 (1997); K. Kutak and J. Kwiecinski, *Eur. Phys. J. C* **29**, 521 (2003); R. Fiore et al., *Phys. Rev. D* **68**, 093010 (2003); M. V. T. Machado, *Phys. Rev. D* **70**, 053008 (2004).
- [28] P. Lipari and T. Stanev, *Phys. Rev. D* **44**, 3543 (1991).
- [29] P. Antonioli, C. Ghetti, E. V. Korolkova, V. A. Kudryavtsev and G. Sartorelli, *Astropart. Phys.* **7**, 357 (1997); I. A. Sokalski, E. V. Bugaev and S. I. Klimushin, *Phys. Rev. D* **64**, 074015 (2001).
- [30] R. M. Sternheimer, M. J. Berger and S. M. Seltzer, *Atom. Data Nucl. Data Tabl.* **30**, 261 (1984).
- [31] A. A. Petrukhin and V. V. Shestakov, *Can. J. Phys.* **46**, S377 (1981).
- [32] S. R. Kelner, R. P. Kokoulin and A. A. Petrukhin, *Phys. Atom. Nucl.* **60**, 576 (1997) [*Yad. Fiz.* **60**, 657 (1997)].
- [33] Based on a parameterization of the HERA data by H. Abramowicz and A. Levy, hep-ph/9712415.
- [34] W. Lohmann, R. Kopp and R. Voss, CERN-85-03.